Supporting Information

Solid-state synthesis of mixed trihalides *via* reversible absorption of dihalogens by non porous onium salts

Lorenzo Meazza,[a] Javier Martí-Rujas,[a] Giancarlo Terraneo,*[a,b] Chiara Castiglioni,[a,c] Alberto Milani,[c] Tullio Pilati,[d] Pierangelo Metrangolo,*[a,b] and Giuseppe Resnati*[a,b,d]

[a] *CNST-IIT@POLIMI, Via Pascoli 70/3, 20133 Milan, Italy.*
[b] *NFMLab, D.C.M.I.C. ''Giulio Natta'', Politecnico di Milano, Via L. Mancinelli 7, 20131 Milan, Italy; Fax: +39 02 2399 3180; Tel: +39 02 2399 3041 (P. M.), 3032 (G. R.), 3036 (G.T.); E-mail: pierangelo.metrangolo@polimi.it , giuseppe.resnati@polimi.it , giancarlo.terraneo@polimi.it.*
[c] *D.C.M.I.C. ''Giulio Natta'', Politecnico di Milano, Piazza L. da Vinci 32, 20133 Milan, Italy.*
[d] ISTM-CNR, via Golgi 19, 20133, Milan, Italy

S1. Experimental

S1.1.General methods: Commercial HPLC-grade solvents were used without further purification. All the reagents were commercially available and used without further purification. Melting points were determined with DSC analyses using Mettler Toledo DSC 823e.

S1.2. General procedure for the synthesis of compounds in solution $1\cdot(Br_2)_2$, $2\cdot(I_2)_2$ and $2\cdot(Br_2)_2$.

S1.2.1. Synthesis of $1\cdot(Br_2)_2$ salt from solution: A solution of Br_2 (0.42 mmol) in methanol (1 mL) was added dropwise to hexamethonium bromide dihydrate (0.28 mmol) in methanol (1 mL) and precipitation occurred giving compound $\mathbf{1\cdot(Br_2)_2}$ as light orange crystals.

S1.2.2. Synthesis of $2\cdot(I_2)_2$ salt from solution: Hexamethonium chloride dihydrate (0.065 mmol) was dissolved in methanol and a solution of I_2 (0.130 mmol) in methanol (1 mL) was added dropwise. After a few minutes brown crystals of $\mathbf{2\cdot(I_2)_2}$ began to precipitate.

S1.2.3. Synthesis of $2\cdot(Br_2)_2$ salt: Hexamethonium chloride dihydrate (0.050 mmol) was dissolved in the minimum amount of methanol and a solution of Br_2 (0.100 mmol) in methanol (1 mL) was added dropwise. Instantaneous precipitation occurred giving dark-orange crystals of $\mathbf{2\cdot(Br_2)_2}$ suitable for X-ray analysis.

S1.3 General procedure for the synthesis of compounds in solid-gas: $1\cdot(Br_2)_2$, $2\cdot(I_2)_2$ and $2\cdot(Br_2)_2$

After the 5 hours of exposure of $\mathbf{1\cdot(H_2O)_2}$ or $\mathbf{2\cdot(H_2O)_2}$ to X_2 gases (Br_2 or I_2), the jar was open to equilibrate with the atmosphere for 24 hours. The same operation was repeated 3 times. The polycrystalline compound $\mathbf{1\cdot(H_2O)_2}$ or $\mathbf{2\cdot(H_2O)_2}$ was occasionally subjected to manual "stirring" to reduce the possibility that different crystallites (e.g., those originally at the top and bottom of the sample) would receive significantly different amounts of X_2 gases exposure within the total duration of the gas-solid reaction.

S.1.4 General procedure for the crystallization of $1\cdot(H_2O)_2$ and $2\cdot(H_2O)_2$

10 mg of purchased $\mathbf{1\cdot(H_2O)_2}$ or $\mathbf{2\cdot(H_2O)_2}$ was put in small vial and was dissolved in 2 mL of methanol. Slow evaporation overnight and at room temperature provided siutable crystals for single crystal X-ray analysis.

S2. X-Ray powder diffraction analyses.

X-ray powder diffraction experiments were carried out on a Bruker D8 Advance diffractometer operating in reflection mode with Ge-monochromated Cu $K\alpha_1$ radiation (λ = 1.5406 Å) and a linear position-sensitive detector. Powder X-ray diffraction data were recorded at ambient temperature, with a 2θ range 5−40°, a step size 0.016°, exposure time 1.5 s per step.

S2.1 Starting materials

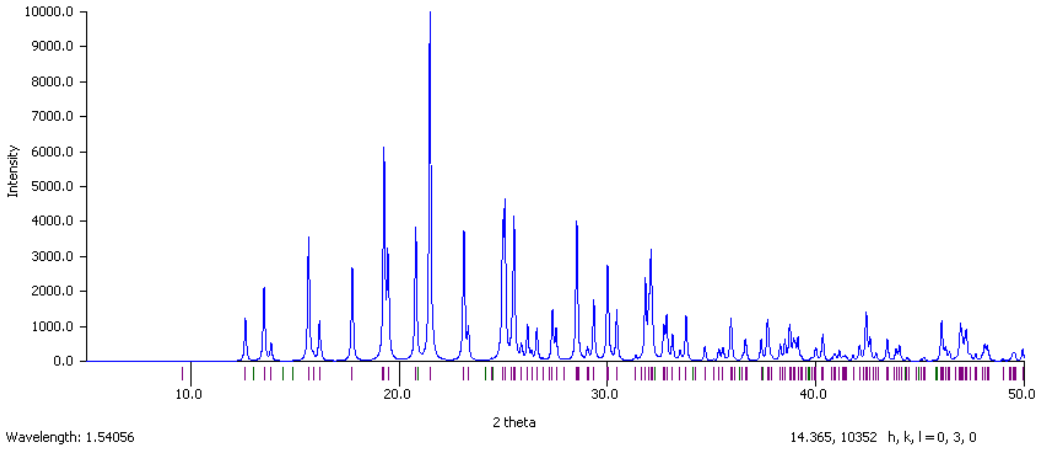

Figure S1: Simulated XRPD of **1**·$(H_2O)_2$.

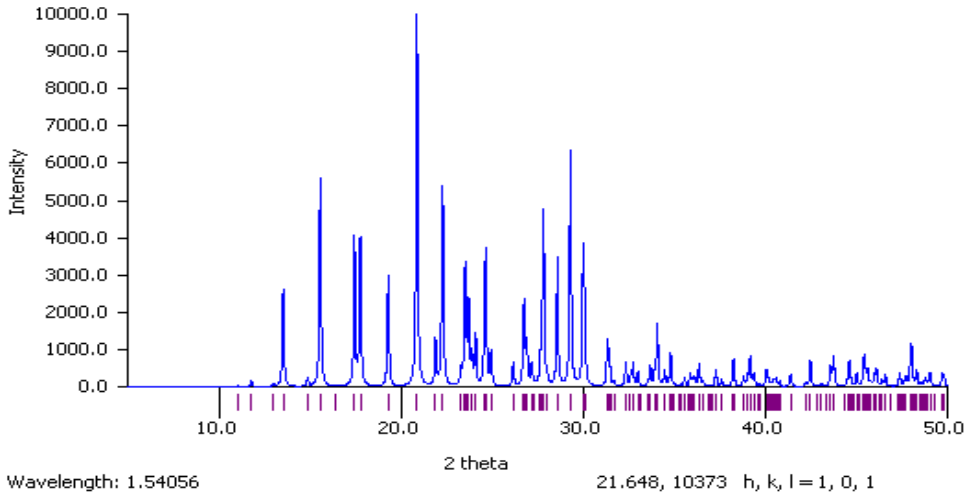

Figure S2: Simulated XRPD of **2**·$(H_2O)_2$.

S2.2 Trihalides

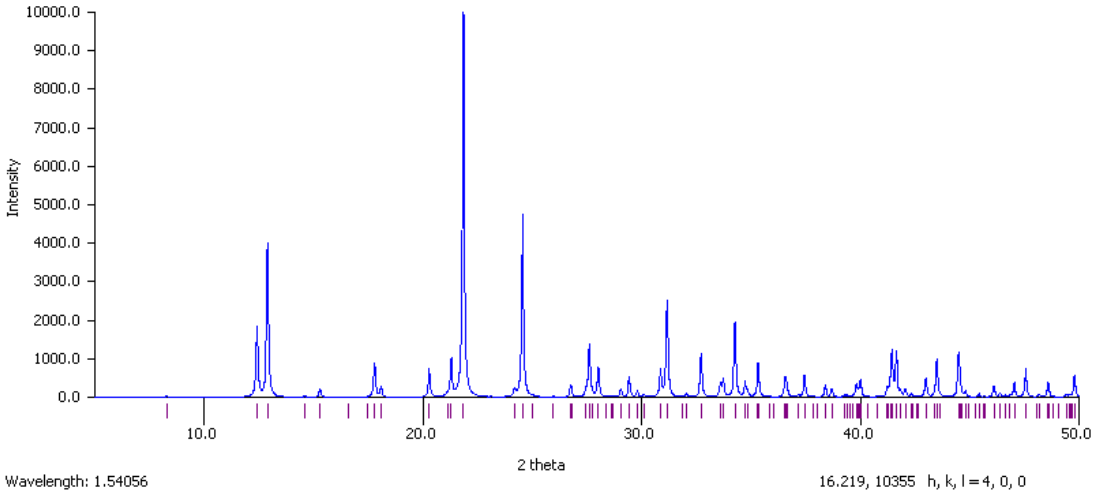

Figure S3: Simulated XRPD of **1·(Br$_2$)$_2$**.

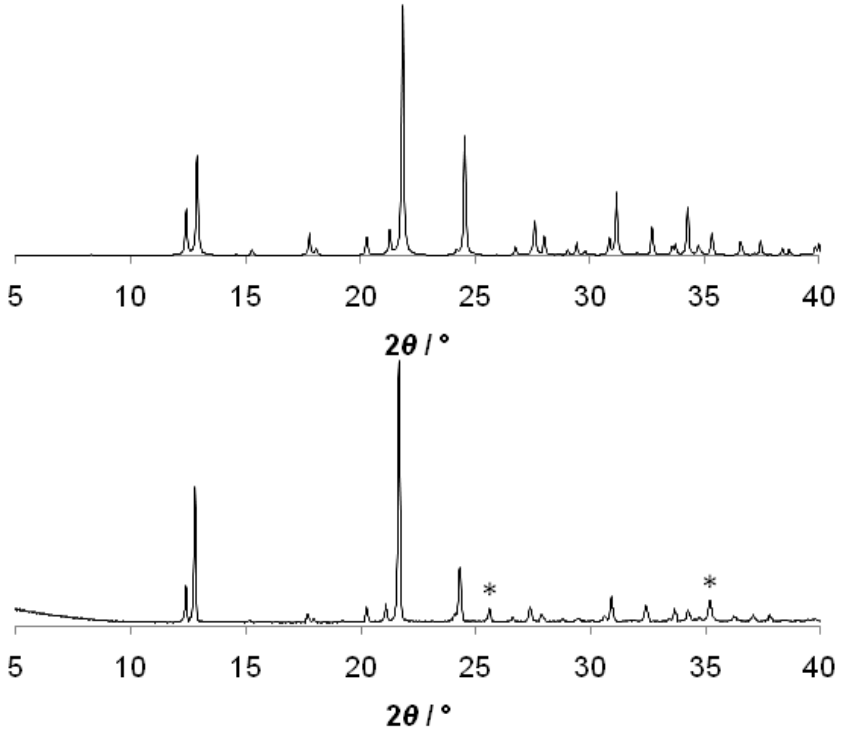

Figure S5: Simulated (top) and experimental (bottom) PXRD patterns of **1·(Br$_2$)$_2$**. The peaks marked with the star mark arise from the presence of Al_2O_3 (internal standard) which was introduced to observe if there was a peak shift in the peaks corresponding of the **1·(Br$_2$)$_2$**.

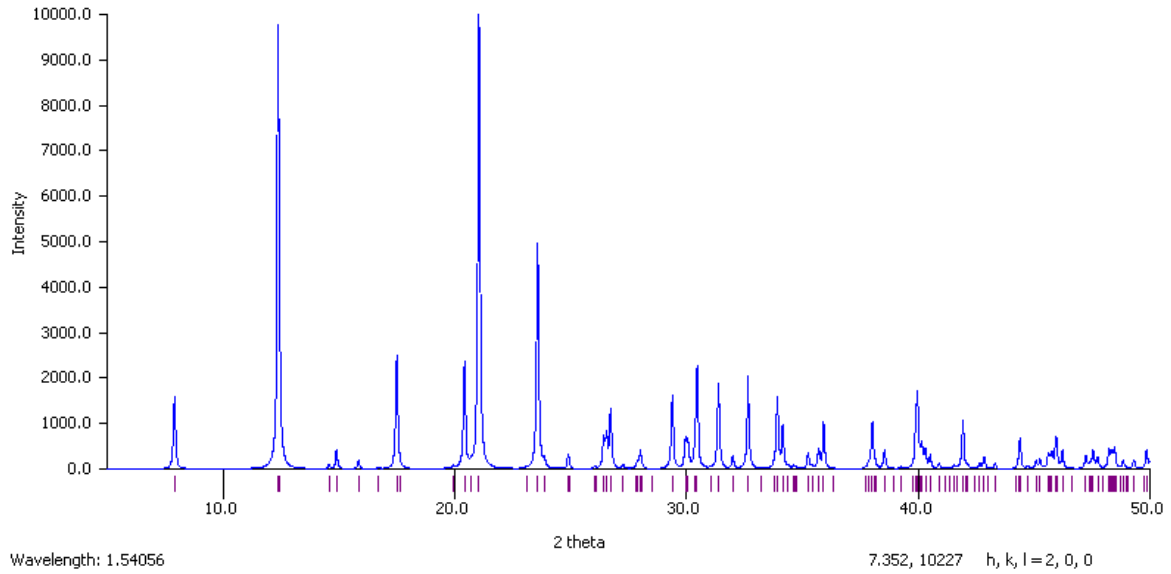

Figure S6: Simulated XRPD of **2**·$(I_2)_2$.

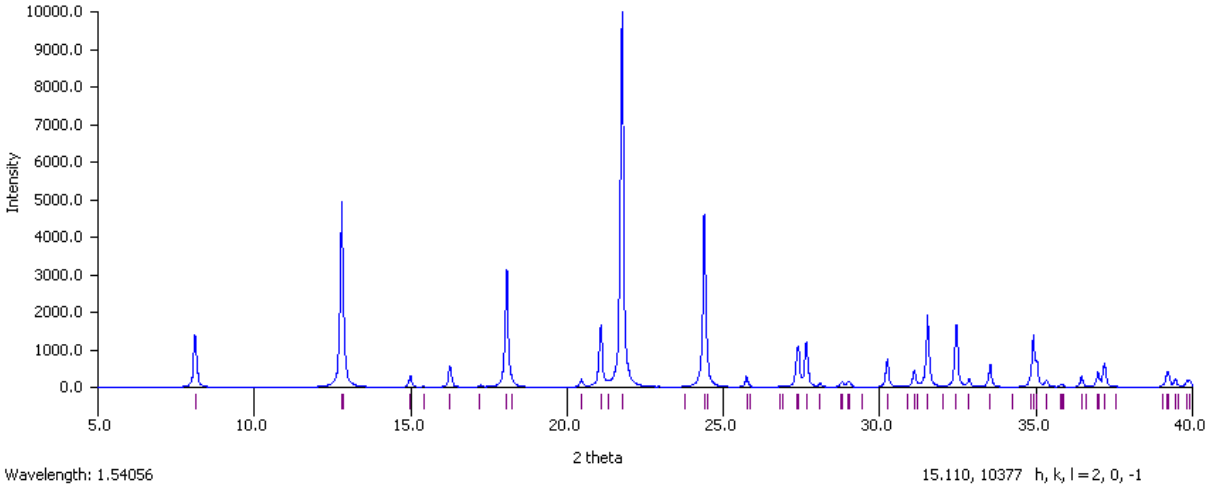

Figure S7: Simulated XRPD of **2**·$(Br_2)_2$.

S2.3. Reversible Inclusion of I_2 and Br_2 in $2\cdot(H_2O)_2$.

S2.3.1 General procedure: 100 mg **$2\cdot(I_2)_2$** or **$2\cdot(Br_2)_2$** was put in a round bottom flask (100 mL) which was attached to a mechanical pump in order to reduce the internal pressure (up to 5 mmHg). The flask was heated for several days and at different temperatures depending of the substrates. Macroscopically, an evidence colour change from coloured powder to white suggested the loss of X_2 and the reversion to **$2\cdot(H_2O)_2$**.

The complete reversion to the starting 1,6-Bis(trimethylammonium)hexane dihydrated bis(halides) was confirmed by XRPD.

$2\cdot(I_2)_2$: Heating at 120°C for 2 days under reduce pressure.

$2\cdot(Br_2)_2$: Heating at 90°C for 2 days under reduce pressure.

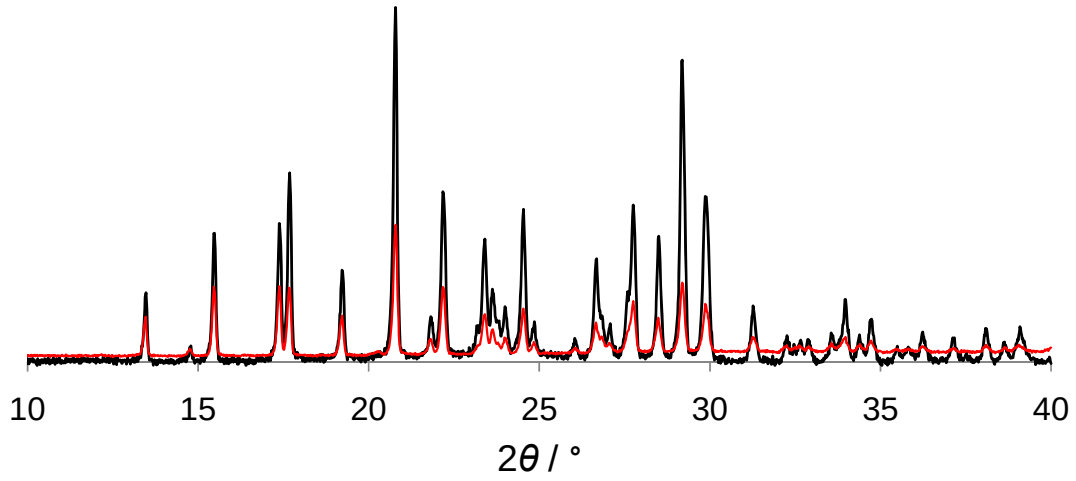

Figure S8: The powder X-ray diffraction after heating to 120 °C in vacuum solid **$2\cdot(I_2)_2$** (red line) overlaps with the diffraction pattern of **$2\cdot(H_2O)_2$** (black).

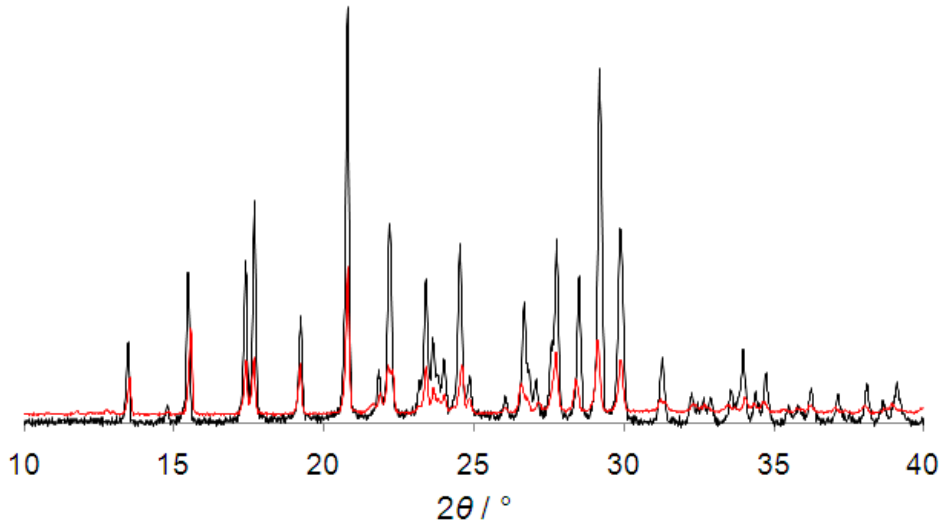

Figure S9: The powder X-ray diffraction after heating to 90 °C in vacuum solid **2·(Br$_2$)$_2$** (red) plotted against the diffraction pattern of **2·(H$_2$O)$_2$** (black).

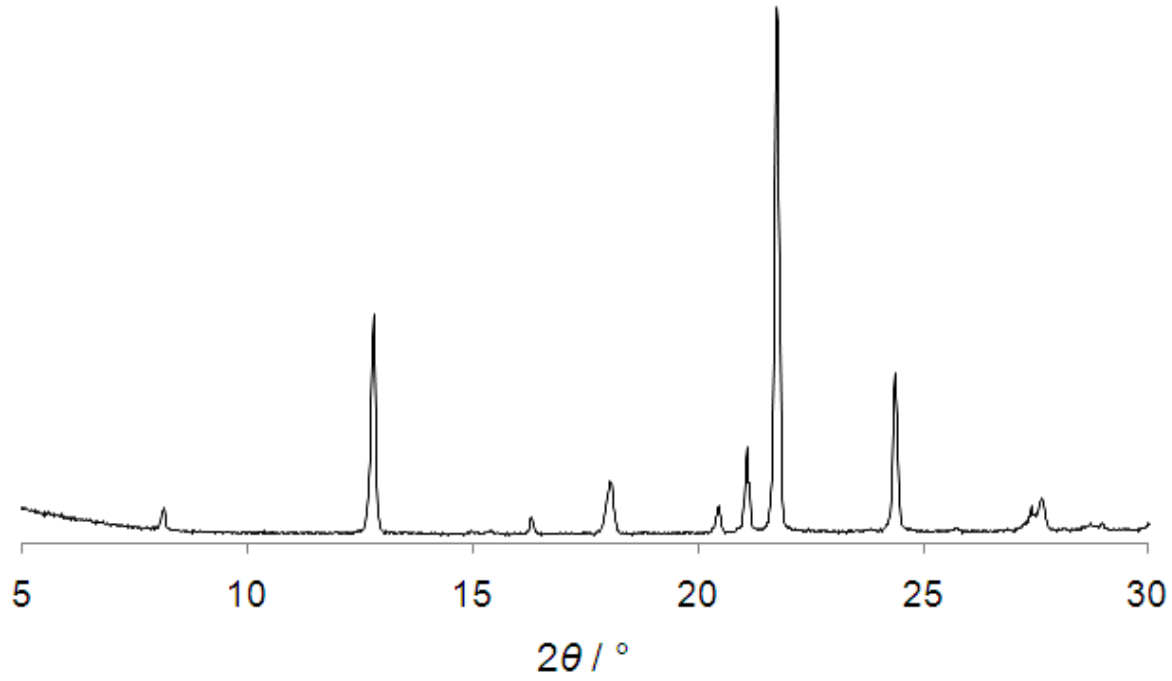

Figure S10: Powder X-ray diffraction after exposing to Br$_2$ **2·(H$_2$O)$_2$** obtained after heating to 90 °C in vacuum solid **2·(Br$_2$)$_2$**. (1 cycle adsorption, release and adsorption of Br$_2$).

S3. X-Ray single crystal diffraction analyses of $1\cdot(H_2O)_2$, $2\cdot(H_2O)_2$, $1\cdot(Br_2)_2$, $2\cdot(I_2)_2$ and $2\cdot(Br_2)_2$.

Single crystal data collection, structure solution and refinement.

Data were collected on a Bruker KAPPA APEX II diffractometer with Mo-Kα radiation and CCD detector. All the crystal structures were collected at room temperature. The structures were solved by SIR2002[1] and refined by SHELXL-97[2] programs, respectively. The refinement was carried on by full-matrix least-squares on F^2. Hydrogen atoms were placed using standard geometric models and with their thermal parameters riding on those of their parent atoms.

These data can be obtained free of charge from The Cambridge Crystallographic Data Centre via www.ccdc.cam.ac.uk/data_request/cif.

[1] M.C. Burla, M. Camalli, B. Carrozzini, G.L. Cascarano, C. Giacovazzo, G. Polidori, R. Spagna. SIR2002: *J. Appl. Cryst.* 2003, **36**, 1103.
[2] G.M. Sheldrick, (1997). SHELXL-97. Program for the Refinement of Crystal Structures. Univ.of Göttingen, German.

Table S1. Single crystal data collection, structure solution and refinement.

Structure	**1·(H$_2$O)$_2$**	**2·(H$_2$O)$_2$**	**1·(Br$_2$)$_2$**	**2·(I$_2$)$_2$**	**2·(Br$_2$)$_2$**
Chemical formula (moiety)	$C_{12}H_{30}N_2^{2+}2(Br^-)$,2(H_2O)	$C_{12}H_{30}N_2^{2+}$ 2(Cl^-), 2(H_2O)	$C_{12}H_{30}N_2^{2+}\cdot2(Br_3^-)$	$C_{12}H_{30}N_2^{2+}\cdot2(I_2Cl^-)$	$C_{12}H_{30}N_2^{2+}$, 1.75(Br_2Cl^-), 0.25(Br_3^-)
Chemical formula (total)	$C_{12}H_{34}Br_2N_2O_2$	$C_{12}H_{34}Cl_2N_2O_2$	$C_{12}H_{14}Br_6N_2$	$C_{12}H_{30}Cl_2I_4N_2$	$C_{12}H_{30}Br_{4.25}Cl_{1.75}N_2$
Formula weight	398.23	309.31	681.84	780.88	604.04
Temperature [K]	103(2)	103(2)	298(2)	298(2)	296(2)
Radiation, wavelength [Å]	MoKα, 0.71073	MoKα, 0.71073	MoKα, 0.71073	MoKα, 0.71073	MoKα, 0.71073
Crystal system, space group	Monoclinic, *P* 21/*c*	Triclinic *P*-1	Monoclinic, *C* 2/*m*	Monoclinic, *C* 2/*m*	Monoclinic, *C* 2/*m*
a [⊕]	7.3339(13)	7.4621(10)	21.450(4)	22.3618(3)	21.800(3)
b [⊕]	18.292(3)	8.1058(11)	7.323(10)	7.5412(12)	7.2927(10)
c [⊕]	7.0915(12)	8.4022(11)	7.1474(11)	7.1251(10)	6.8951(10)
α [°]	90.00	94.013(10)	90.00	90.00	90.00
β [°]	108.824(4)	116.002(12)	92.31(2)	91.388(12)	91.743(12)
γ [°]	90.00	99.107(11)	90.00	90.00	90.00
Cell volume [Å^3]	900.4(3)	445.42(10)	1121.8(3)	1201.1(3)	1095.7(3)
μ_{calc} [g cm-1]	1.469	1.153	2.019	2.159	1.831
Z	2	1	2	2	2
dimension [mm^3]	0.06 x 0.16 x 0.32	0.14 x 0.28 x 0.36	0.02 x 0.18 x 0.19	0.11 x 0.13 x 0.22	0.04 x 0.12 x 0.14
μ(MoKα) [mm^{-1}]	4.501	0	10.732	5.407	8.010
F(000)	412	170	652	724	589
Crystal colour and shape	Colourless table	Colourless block	Orange-yellow table	Purple table	Orange table
θ_{max} [°]	30.24	32.70	30.56	30.47	26.42
Data collected	30772	9178	7088	7261	18315
Unique data	2604	2997	1804	1910	1223
R_{int}	0.0286	0.0225	0.0391	0.0228	0.0317
No. obs. data *Io*>2σ(*Io*)]	2412	2786	1036	1453	890
no. parameters	93	150	67	59	60
No. Restrains.	0	0	0	0	0
R_{all}	0.0200	0.0253	0.0751	0.040	0.0428
R_{obs}	0.0172	0.0232	0.0328	0.0266	0.0243
wR_{all}	0.0453	0.0628	0.0869	0.0646	0.0563
wR_{obs}	0.0441	0.0617	0.0723	0.0594	0.0509
Goodness-of-fit on F^2	1.088	1.071	1.001	1.047	1.047

$\Delta\rho_{min,max}$ [e Å^{-3}]	-0.393; 0.381	-0.300; 0.416	-0.389, 0.765	-0.652, 0.690	-0.278, 0.320
CCDC	797580	797581	797582	797583	801987

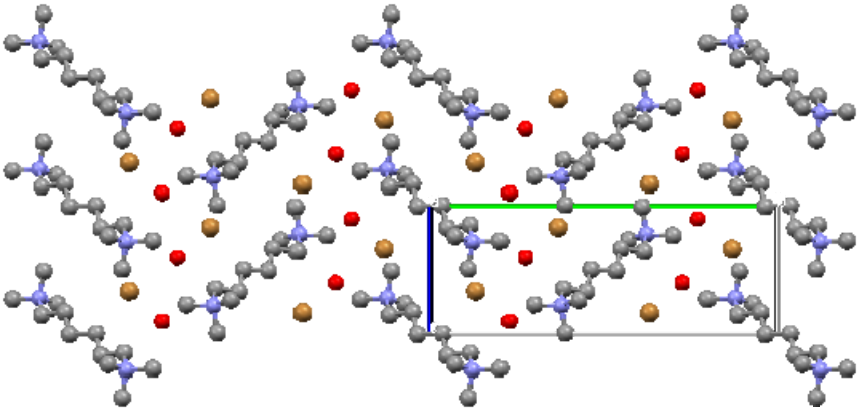

Figure S11: Crystal structure of **1·(H$_2$O)$_2$.** The water molecules interact with the Br atoms through a hydrogen bonding interaction. Hydrogen atoms are omitted for clarity.

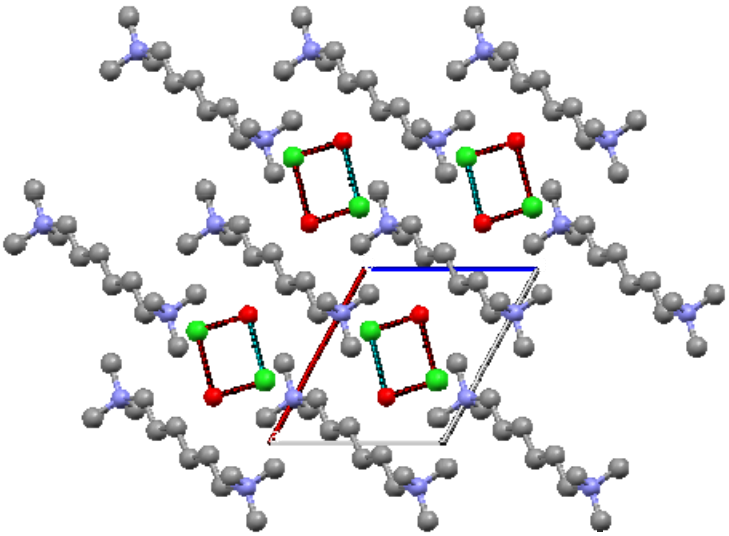

Figure S12: Crystal structure of **2·(H$_2$O)$_2$**. The water molecules interact with the Cl atoms through a hydrogen bonding interaction. Hydrogen atoms are omitted for clarity.

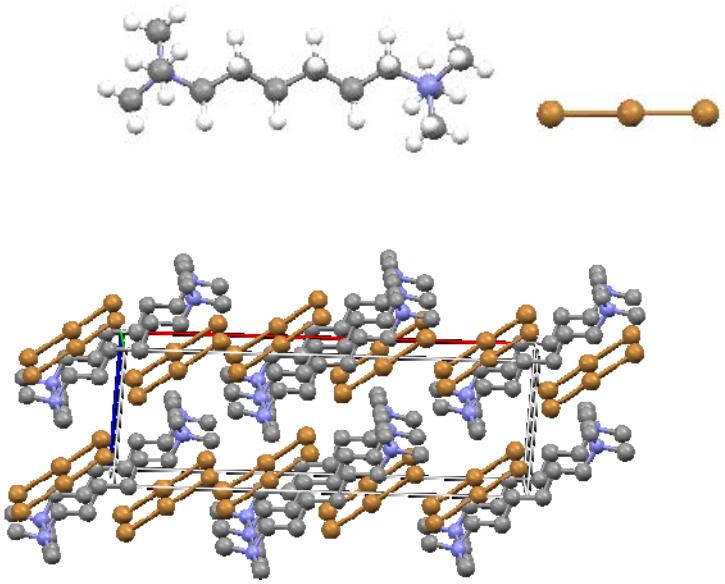

Figure S13: Crystal structure of **1·(Br$_2$)$_2$**. Asymmetric unit (top) and packing of cations and anions in the unit cell viewed approximately along the *b* crystallographic axis (bottom).

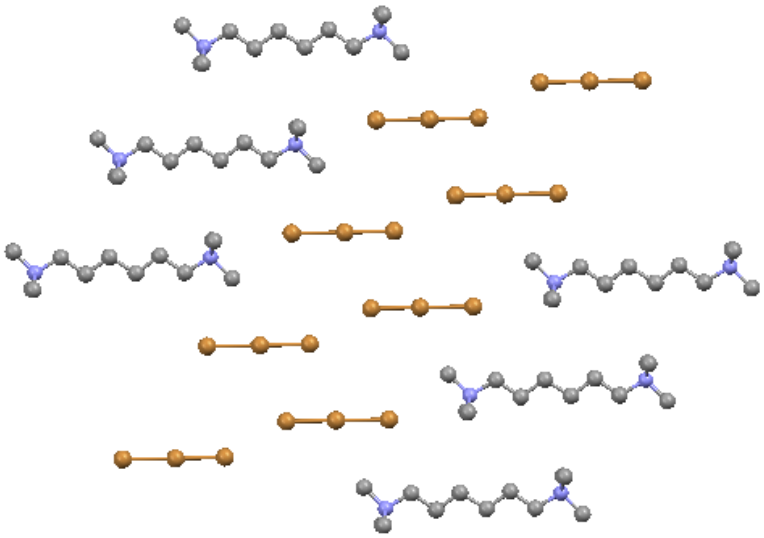

Figure S14: Array of **Br$_3^-$** along the *c* axis showing the distances between superanions (dashed line).

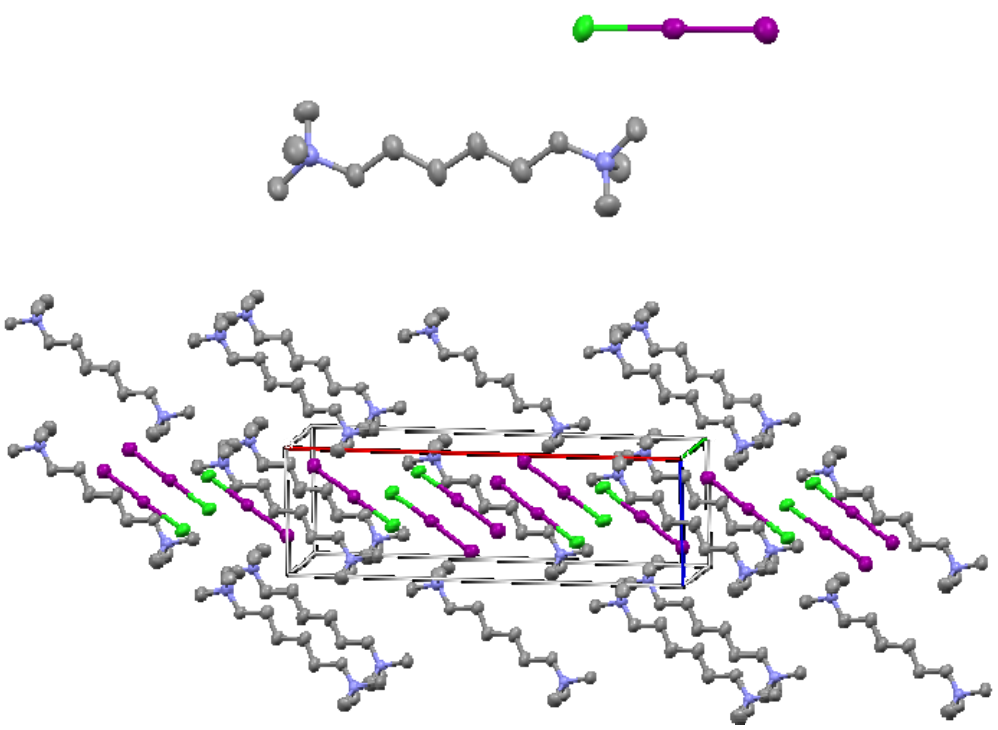

Figure S15: Crystal structure of **2**·$(I_2)_2$. Asymmetric unit (top) and packing of unit cell viewed approximately along the *b* crystallographic axis (bottom).

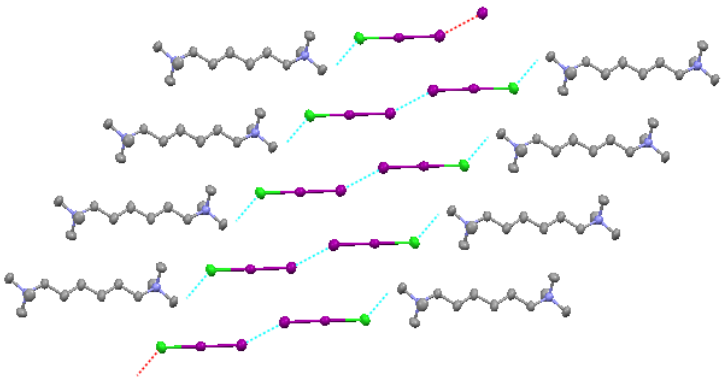

Figure S16: Array of **2**·$(I_2)_2$ along the *c* axis showing the short contacts between superanions (dashed line).

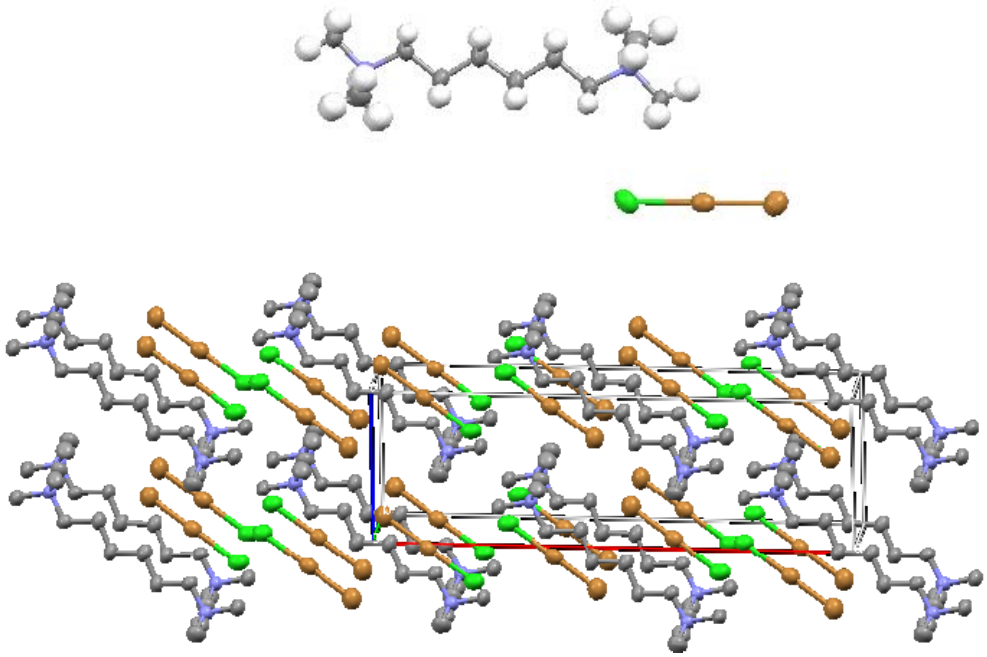

Figure S17: Crystal structure of **2·(Br$_2$)$_2$**. Asymmetric unit (top) and packing of unit cell viewed approximately along the *b* crystallographic axis (bottom).

S.4. Raman Analysis

FT-Raman spectra have been recorded with a Nicolet NXR 9650 Raman Spectrometer in a backscattering geometry on samples prepared in capillary glass tube. The line at 1064 nm of a Nd:YVO4 laser was used as exciting source; to prevent possibly degradations the beam diameter was kept defocused (1 mm diameter) with a power measured on the samples of 260 mw. For every spectrum 512 scansions have been acquired and averaged.

Table S2: Frequency, Raman intensity and vibrational assignment

Trihalides	Model[a]	Frequency (cm^{-1})	Raman Intensity (A^4/amu)	Vibrational Assignment
Br_3^-	1	138 201	26 22	//
	2	144 207	118 279	Br-Br (long bonds) symm. stretching Br-Br (short bonds) symm. stretching
	3	151 198	4 106	//
Br_2Cl^-	1	158 221	28 36	//
	2	173 225	86 269	Br-Cl symm. stretching Br-Br symm. stretching
I_2Cl^-	1	171 176	52 9	//
	2	170 193	503 1	I-I symm. stretching I-Cl symm. stretching

[a] model 1) an isolated Br_3^- anion; model 2) a dimer of interacting Br_3^- anions, namely $(Br_3^-)_2$; model 3) a Br_3^- anion interacting with small models of the organic cations (hydrogen bonding).

DFT computed[3] (PBE1PBE/aug-cc-pVTZ + ECP28MDF for I atoms) frequencies (cm^{-1}) and Raman intensities (A^4/amu) for the molecular models of Br_3^-, Br_2Cl^- and I_2Cl^- crystals. The vibrational assignment is reported for the case of models II, adopted in the interpretation of the experimental FT-Raman spectra.

It must be noticed that in the case of models II the Raman intensities reported in column four are normalized on a single trihalide molecule to be compared correctly with the intensities calculated in the other cases (where only one trihalide molecule is indeed present).

[3] Gaussian 03, Revision C.02, M. J. Frisch, G. W. Trucks, H. B. Schlegel, G. E. Scuseria, M. A. Robb, J. R. Cheeseman, J. A. Montgomery, Jr., T. Vreven, K. N. Kudin, J. C. Burant, J. M. Millam, S. S. Iyengar, J. Tomasi, V. Barone, B. Mennucci, M. Cossi, G. Scalmani, N. Rega, G. A. Petersson, H. Nakatsuji, M. Hada, M. Ehara, K. Toyota, R. Fukuda, J. Hasegawa, M. Ishida, T. Nakajima, Y. Honda, O. Kitao, H. Nakai, M. Klene, X. Li, J. E. Knox, H. P. Hratchian, J. B. Cross, V. Bakken, C. Adamo, J. Jaramillo, R. Gomperts, R. E. Stratmann, O. Yazyev, A. J. Austin, R. Cammi, C. Pomelli, J. W. Ochterski, P. Y. Ayala, K. Morokuma, G. A. Voth, P. Salvador, J. J. Dannenberg, V. G. Zakrzewski, S. Dapprich, A. D. Daniels, M. C. Strain, O. Farkas, D. K. Malick, A. D. Rabuck, K. Raghavachari, J. B. Foresman, J. V. Ortiz, Q. Cui, A. G. Baboul, S. Clifford, J. Cioslowski, B. B. Stefanov, G. Liu, A. Liashenko, P. Piskorz, I. Komaromi, R. L. Martin, D. J. Fox, T. Keith, M. A. Al-Laham, C. Y. Peng, A. Nanayakkara, M. Challacombe, P. M. W. Gill, B. Johnson, W. Chen, M. W. Wong, C. Gonzalez, and J. A. Pople, Gaussian, Inc., Wallingford CT, 2004.

S.4.1. Raman details for 2. Br_2Cl^-/Br_3 sample

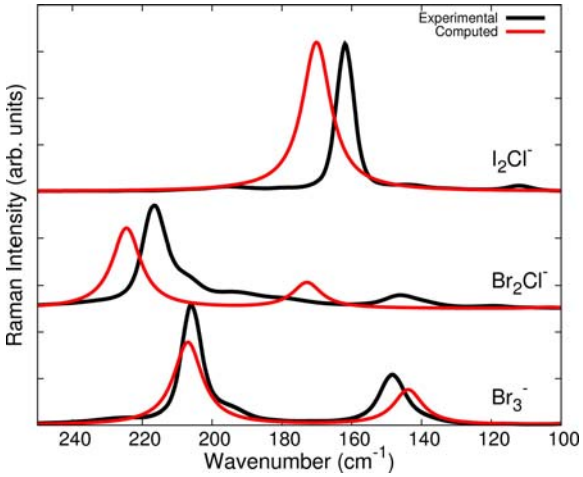

Figure S18: Experimental FT-Raman spectra (black lines) of Br_3^-, Br_2Cl^-, and I_2Cl^- in crystals **1·(Br$_2$)$_2$**, **2·(Br$_2$)$_2$**, and **2·(I$_2$)$_2$** and DFT computed Raman spectra of related models.

Notice that the theoretical prediction for $(Br_2Cl^-)_2$ is compared in Figure S18 to the experimental spectrum obtained for a crystal with a Br_2Cl^-/Br_3^- ratio of 7/1: this is the origin of the many spectral components observed. Indeed, simply looking to the experimental spectrum of the Br_3^- crystal, the lower frequency feature can be assigned to the Br_3^- transition (~150 cm^{-1}), while the markedly asymmetric shape shown by the higher frequency band is certainly due to the contribution of the Br_3^- line at ~205 cm^{-1}